https://doi.org/10.1016/j.engstruct.2021.112360

Structural performance of concrete-filled cold-formed high-strength steel octagonal tubular stub columns

Han Fang[1], Tak-Ming Chan[2,3]* and Ben Young[2]

[1]School of Civil, Environmental and Mining Engineering, The University of Adelaide, South Australia 5005, Australia

[2]Department of Civil and Environmental Engineering, The Hong Kong Polytechnic University, Hong Kong, China

[3]Chinese National Engineering Research Centre for Steel Construction (Hong Kong Branch), The Hong Kong Polytechnic University, Hung Hom, Hong Kong, China

*Corresponding author: tak-ming.chan@polyu.edu.hk

Abstract

This paper presents a comprehensive experimental and numerical study on the structural performance of concrete-filled cold-formed high-strength steel octagonal tubular stub columns. Stub column specimens formed using high-strength steel and infilled concrete with grades C50 and C90, and with three different plate width-to-thickness ratios were tested. The ultimate loads, load-displacement responses and failure modes of the structures were observed and discussed. In addition to the experimental investigations, a finite element model validated using the stub column test results was developed. A series of parametric studies were subsequently conducted to obtain supplementary data for concrete-filled cold-formed high-strength steel octagonal tubular stub columns with a wide range of plate width-to-thickness ratios and different concrete compressive strengths. The applicability of existing design approaches in European and American standards and in literature provided for concrete-filled steel tubular structures with rectangular, circular or octagonal cross-sections were evaluated using the results obtained from the experimental and numerical study. The accuracy of design predictions for concrete-filled cold-formed high-strength steel octagonal tubular stub columns using different design approaches was discussed. A design approach that more accurately incorporates the strength contributions from steel tubes and concrete infill was also proposed for structural design.

Keywords: Concrete-filled steel tubes, cold-formed, octagonal cross-section, stub columns, high-strength steel, testing, numerical study, structural design.

1. Introduction

Concrete-filled steel tubular (CFST) structures have been increasingly applied in composite construction of buildings and bridges owing to their high structural capacity and ductility, energy dissipation performance and fire resistance [1-4]. Besides the high structural performance, the outer steel tubes are used as the formwork for concrete casting, resulting in faster and more economical construction [5-6]. Comprehensive research studies have been performed to investigate the behaviour of CFST structures formed using normal strength materials and under various loading conditions that can occur to the structures in applications [3, 5, 7-11]. With the developments of material manufacture and concrete technology, high-strength steel (HSS) with nominal yield strength above 460MPa and high-strength concrete (HSC) with cylinder compressive strength above 70MPa are available to obtain stronger and lighter structures [12-17] and have received wide interests for their use to form CFST structures [6, 17-19]. During recent years, effective research progresses have been achieved on CFST structures made of high-strength materials and with circular and rectangular cross-sections [6, 10, 17-18, 20-21]. For these structures, the circular shape steel tubes provide more effective confinement to the concrete infill while rectangular shape steel tubes for CFST members provide flat surfaces to allow easier construction of joints connecting incoming members with the CFST members. Comparing with circular and rectangular CFST structures, octagonal shaped cross-sections have recently been found to provide combined high confinement from the outer octagonal steel tube and flat surfaces for connection construction [22].

Despite the advantages of CFST structures with octagonal cross-sections, limited studies were performed to examine the performance of the structures. Tomii et al. [23] tested nine octagonal CFST stub columns with three cross-sectional sizes and the stub columns were made of conventional strength steel with yield strength (f_y) of about 294.3-341.3MPa and conventional strength concrete with cylinder compressive strength (f_c) of 16.7-30.1MPa. Ding et al [24] tested eight octagonal CFST stub columns with three cross-sectional sizes and formed using conventional strength steel with f_y of about 311-321 MPa and concrete with cubic compressive strength (f_{cu}) of 39.3 and 57.4MPa. Hassamnein et al [25] investigated octagonal CFST stub columns formed using conventional strength steel with f_y of about 350MPa and conventional strength concrete and HSC with f_c of 40-100MPa. In the study, it was also suggested that strength predictions with reasonable accuracy was obtained based on the design approach for circular CFST stub columns in Eurocode 4 [26]. Zhu and Chan [22, 27] investigated octagonal CFST stub columns made of conventional strength steel with f_y of 296.3-413MPa and conventional strength concrete and HSC with f_c of 37.7-113.5MPa. Zhu and Chan [22] also found that conservative strength predictions were obtained using the design approaches given in Eurocode 4 and AISC 360 [28] for rectangular CFST stub columns and proposed an approach based on the obtained experimental results for octagonal CFST stub columns with conventional strength

steel. Based on the above research results for octagonal CFST stub columns, Ahmed and Liang [29] performed numerical modelling and evaluated design approaches in standards. It was also found that overestimation of structural capacities was obtained based on the design approach in Eucocode 4 [26] for circular sections while conservative predictions was obtained based on AISC 360 standard [28]. These existing research studies mostly focused on the octagonal CFST stub columns with conventional strength steel. Limited attention has been paid to the octagonal CFST stub columns made of HSS.

Therefore, a comprehensive study through experiments and numerical modelling was performed on the concrete-filled cold-formed HSS (CFHSS) octagonal tubular stub columns. Experiments were performed to investigate the behaviour of concrete-filled CFHSS octagonal tubular stub columns made of different concrete grades and with cross-sectional sizes. A numerical study was performed, in which a validated finite element model based on experimental results was developed and subsequently applied to carry out parametric studies on the concrete-filled CFHSS octagonal tubular stub columns with various dimensions and material strengths. The obtained experimental and numerical results were also compared with the strength predictions based on specifications given in Eurocode 4 and AISC 360 and the approaches proposed by Zhu and Chan [22] and Ahmed and Liang [29] so that the applicability of the design approaches to the structures investigated in the current study was evaluated. Finally, a design approach with improved accuracy is proposed.

2. Experimental investigation

2.1 Specimens and material properties

CFHSS octagonal tubular stub column specimens with and without concrete infill were prepared for experimental investigations, as summarised in Table 1 based on the nomenclature described in Fig. 1. The CFHSS octagonal tubes for these specimens were fabricated using S690 plates with nominal yield strength and thickness of 690MPa and 6mm respectively. In the table, the specimens were labelled based on the tube size and concrete grade. For example, the Oct-50×6-C50a defines the specimen with respective nominal steel tube side length and thickness of 50mm and 6mm and made of C50 concrete with nominal f_c of 50MPa. The last segment “a” or “b” was used to distinguish the specimens with the same nominal dimensions and concrete grade. The specimens labelled with “C0” are the CFHSS octagonal tubular stub columns without concrete infill. The CFHSS octagonal tubes for the specimens were fabricated by press-braking HSS plates into half-sections and subsequent welding of two half-sections, as shown in Fig. 1. The specimens were prepared using CFHSS octagonal tubes with three plate width-to-thickness ratios. For the specimens with the same nominal tubular cross-section size, concrete with different grades of C50 and C90 with nominal f_c of 50MPa and 90MPa respectively were prepared and poured into the tubes to form the concrete-filled CFHSS

98 octagonal tubular stub columns. The nominal length (L) of each specimen was taken as three times of
99 the width (D) shown in Fig. 1 of the specimen cross-section. The dimensions of the specimens were
100 measured and provided in Table 1.

101 The material properties of CFHSS octagonal tubular sections for the specimens are required for
102 subsequent numerical study and evaluation of design approaches. The tubes for the current study were
103 obtained using the HSS plates in the same batch as those used for fabricating the CFHSS octagonal
104 tubular structures investigated in previous studies [30-32]. The detailed measurements of properties of
105 materials at the flat and corner regions across the CFHSS octagonal tubular sections have been
106 presented in those previous studies, and thus, key results as the average values of material properties
107 at the flat and corner regions are summarized here in Table 2 while the typical stress-strain curves
108 from the measurements are given in Fig. 2. In Table 2, E_s, $\sigma_{0.2}$, σ_u, ε_u and ε_f represent the elastic
109 modulus, 0.2% proof stress, ultimate tensile strength, ultimate tensile strain, and elongation at fracture,
110 respectively.

111 Concrete grades of C50 and C90 grades were prepared in the laboratory using the mix proportions
112 shown in Table 3. Nine concrete cylinder specimens with the standard size of 150×300mm for each
113 concrete grade were also prepared in parallel to the process of pouring concrete for the concrete-filled
114 stub columns specimens. Both concrete-filled CFHSS octagonal tubular stub columns and concrete
115 cylinder specimens were cured under the same environmental conditions. The cylinders were tested
116 during the test days of the stub columns and the average f_c of the C50 and C90 concrete were obtained,
117 as presented in Table 3.

118 **2.2 Stub column tests**

119 The stub columns were tested under axial compression using a 10,000kN loading machine, as shown
120 in Fig. 3 for the test set-up. To obtain flat end surfaces for uniform loading during the tests, plaster
121 material was applied to fill the small gap at the top surface between the steel tube and concrete infill
122 [17, 33] for concrete-filled CFHSS octagonal tubular stub column specimens. The end surfaces of
123 Oct-50×6-C0, Oct-70×6-C0 and Oct-85×6-C0 specimens without concrete infill were also milled flat
124 before testing. In order to avoid premature failure at the specimen ends, steel rings as end stiffeners
125 were fixed near the two ends of each specimen [22, 31, 33], as highlighted in Fig. 3. The end-
126 shortening (δ) of the specimens was measured using three linear variable displacement transducers
127 (LVDTs). Strain gauges were attached to the middle of the flat and corner portions in both
128 longitudinal and transverse directions to measure the local strain developments along with increasing
129 compression. During each test, the axial compressive loading was applied through the displacement
130 control at a rate of 0.25mm/min so that the test continued after the ultimate load was obtained.

2.3 Test results

The behaviour of the stub column specimens under axial compression was observed during the tests. The load versus δ responses are shown in Fig. 4 for different stub column specimens while the ultimate load ($P_{u,exp}$) obtained for each test specimen is provided in Table 1. The δ in Fig. 4 was obtained as the average of the measurements from three LVDTs during each test. As can be observed in the figure, with the same nominal CFHSS octagonal tubular cross-section size, higher $P_{u,exp}$ of 43-103% were obtained for the specimens with concrete infill of C50 and C90 grades respectively. Besides, with increasing f_c for each cross-sectional sizes, reductions in ductility of the concrete-filled CFHSS octagonal tubular stub columns were observed from the load versus δ curves in Fig. 4 due to the higher concrete brittleness and the load dropped more rapidly after the $P_{u,exp}$ were reached. In Fig. 4(b), it can also be seen that the curve for the Oct-70×6-C90b specimen experienced a different pattern for the post-ultimate stage. After the $P_{u,exp}$ was reached, the load for the Oct-70×6-C90b specimen initially decreased faster than that for the Oct-70×6-C90a specimen. This observation may be the consequence of the local buckling occurrence due to a larger local geometric imperfection in the CFHSS octagonal tube of the Oct-70×6-C90b specimen.

It can also be observed in the Fig. 4 that the compressive stiffness for the concrete-filled CFHSS octagonal tubular stub columns is generally larger than that for the stub columns without concrete infill since the compressive stiffness is contributed from the elastic modulus and cross-sectional area of steel tube and concrete infill [3]. The increment of compressive stiffness in comparison with the CFHSS octagonal tubular stub columns is relatively lower for the Oct-50×6-C50a, Oct-50×6-C50b, Oct-50×6-C90a, and Oct-50×6-C90b specimens. This observation is obtained since these specimens have the relatively small cross-sectional area of concrete infill in proportion to that for steel tube and the elastic modulus of steel is much higher than that for concrete.

Load versus strain relationship was also recorded and obtained through the stub column tests, as plotted in Fig. 5 for different specimens. Both longitudinal and hoop strains in the middle of flat and corner regions at mid-height of the specimens were measured and are shown in the figure. As can be seen in the figures, the load initially increases linearly with increasing strains in the elastic stage. The strains at the flat and corner portions were approximately the same. After the loads increased up to about 70-80% of $P_{u,exp}$ of the CFST stub columns, the strains increased more rapidly. At these higher loads, the longitudinal strains at different locations increased with consistent trends. For the hoop strains at the higher loads, the strain at the corner region was lower than that at the flat region at the same load level. The observation for hoop strains was caused by the relatively higher concrete expanding with lower confinement at the flat region in comparison with the confinement at the corner region. Since these strain results were obtained from measurements at mid-height, these strains may

not reflect the strain developments at the locations where local buckling of each specimen occurred after the $P_{u,exp}$ was reached.

The failure modes of the stub column specimens were also observed during testing. For the Oct-50×6-C0, Oct-70×6-C0 and Oct-85×6-C0 specimens, yielding failure mode was observed since these specimens have relatively small B/t ratios and lower than the slenderness limit beyond which elastic local buckling occurs [31, 34]. As for the concrete-filled CFHSS octagonal tubular stub columns, the failure mode of the structures was found as the crushing of concrete infill with the outward local buckling of the outer CFHSS octagonal tubes, as shown in Fig. 6. As the B/t ratios for the specimens are relatively lower, the local buckling mainly occurred after the $P_{u,exp}$ of each specimen was reached.

3. Numerical investigation

3.1 General

Numerical modelling using the finite element analysis package ABAQUS 6.14 was also performed to investigate the behaviour of concrete-filled CFHSS octagonal tubular stub columns with a wide range of parameters to supplement the experimental investigation. The finite element (FE) model was developed incorporating the material properties, boundary conditions and composite interaction between the CFHSS octagonal tube and concrete infill of each structure. The FE model and its validation using the results from stub column tests are provided in the following sections.

3.2 Description of the FE model

The structures were simulated using shell elements S4R for the CFHSS octagonal tubes [12, 31, 35] and solid elements C3D8R for the concrete infill [17, 36-37]. Through convergence studies, the element mesh size of $B/10$ for steel and concrete infill was adopted. To accurately replicate the stub column test results, the measured material properties for CFHSS octagonal tubular cross-sections through tensile coupon tests were employed as the input of the FE model. The measured stress-strain relationship for flat and corner regions were converted into true stress versus log plastic strain relationship which was subsequently incorporated in the FE model for the respective regions.

The properties of concrete infill for concrete-filled CFHSS octagonal tubular stub columns was incorporated in the model using the concrete damage plasticity (CDP) model in ABAQUS [38]. The elastic modulus (E_c) of concrete infill was estimated as $4700\times f_c^{0.5}$ [39-40] while the Poisson's ratio was taken as 0.2. The stress-strain model provided by Han et al [41] for concrete infill in circular steel tubes was adopted for the FE model in this study, considering the better confinement performance obtained for octagonal CFST stub columns than square CFST stub columns [22]. The suitability of the model was evaluated through the validation described in Section 3.3. Other parameters required for

the CDP model include the dilation angle (ψ), flow potential eccentricity (e), the ratio of the compressive strength under biaxial loading to uniaxial compressive strength (f_{b0}/f_{ck}), the ratio of the second stress invariant on the tensile meridian to that on the compressive meridian (K_c) and viscosity parameter. The ψ was estimated using the method suggested by Tao et al [42], as given in Eq. (1). The ξ in Eq. (1) is confinement factor and defined in Eq. (2), where A_s and A_c are the cross-sectional areas of CFHSS octagonal tubular sections and concrete infill, respectively. Default values of 0.1 and 0 for e and viscosity parameter respectively were used. The f_{b0}/f_{ck} for the structures was calculated from Eq. (3) provided by Papanikolaou and Kappos [43]. The parameter K_c was estimated using Eq. (4) [42, 44] for each concrete-filled CFHSS octagonal tubular stub column and incorporated into FE model. Apart from the aforementioned parameters, tensile properties were also defined in the model. The tensile strength equals to $0.1f_c$ while the fracture energy (G_f) estimated using Eq. (5) [42, 45] was used in the model. In Eq. (5), the d_{max} is the maximum coarse aggregate size in mm and equals to 20mm.

$$\Psi = \begin{cases} 56.3 \times (1-\xi)\ for\ \xi \le 0.5 \\ 6.672 \times e^{\frac{7.4}{4.64+\xi}}\ for\ \xi > 0.5 \end{cases} \quad (1)$$

$$\xi = \frac{A_s \times f_y}{A_c \times f_c} \quad (2)$$

$$f_{b0}/f_{ck} = 1.5/f_c^{0.075} \quad (3)$$

$$K_c = \frac{5.5}{5+2f_c^{0.075}} \quad (4)$$

$$G_F = (0.0469 d_{max}^2 - 0.5 d_{max} + 26)\left(\frac{f_c}{10}\right)^{0.7} \quad (5)$$

Besides the consideration of material properties, interaction between the outer CFHSS octagonal tube and the concrete infill of each concrete-filled CFHSS octagonal tubular stub column was also taken into account. Surface-to-surface contact was defined at the interface of the tube and concrete infill of each stub column. “Hard contact” was specified in the normal direction while the Coulomb friction model was applied in the tangential direction. Friction coefficients of different values from 0.25 to 0.6 were used in literature [9, 17, 33, 36-37, 41]. In the current study, the friction coefficient of 0.25 was adopted through performing a sensitivity analysis. Initial geometric imperfections and residual stresses exist in CFHSS octagonal steel tubes [30-31]. They can influence the performance of steel tubular cross-sections under compression and are incorporated in the FE model for stub columns without concrete infill (Oct-50×6-C0, Oct-70×6-C0 and Oct-85×6-C0) following the arrangements introduced in previous studies on the structural performance of CFHSS octagonal steel tubular stub columns [31-32]. As for stub columns with concrete infill, the influence of initial geometric

imperfections and residual stresses was found to be quite limited due to the presence of concrete infill [33, 42], and thus were not incorporated in the FE model for the structures.

Boundary conditions were also applied using the reference points according to the test set-up arrangements. Each reference point was located in the middle of the end cross-section of each stub column and coupled with the corresponding end cross-section. At the reference points, all degrees of freedom were restrained except for the longitudinal translation. The compressive loading was applied by specifying the axial displacement at the reference point on the loaded side in a Static step adopted to predict the structural behaviour of the stub columns.

3.3 Validation of FE model

The FE model described in the previous section was validated against the results of stub column tests. The ultimate loads ($P_{u,FE}$) predicted by the FE modelling were compared with the experimental results in Table 1. The $P_{u,FE}$ agreed well with the $P_{u,exp}$ for the stub column specimens, as observed in Table 1. The mean value of $P_{u,FE}/P_{u,exp}$ ratios is 0.99 with the Coefficient of Variation (CoV) as 0.04. The FE modelling results of load versus δ responses were also plotted and compared with the experimental results in Fig. 7 for typical specimens. It is clearly revealed in the figure that the load versus δ responses are accurately replicated by the FE modelling. Fig. 8 is also presented and shows the capture of the structural failure mode. Overall, the FE model developed in this study is validated with the capability of accurately predicting the behaviour of the stub column specimens.

3.4 Parametric studies

The validated FE model was used to perform parametric studies on the behaviour of concrete-filled CFHSS octagonal tubular stub columns with various cross-sectional dimensions giving different B/t ratios and strength of concrete infill (concrete grades). Varying B values were selected to obtain B/t ratios ranging from 8 to 50 (B/t = 8, 15, 20, 25, 30, 35, 40, 45 and 50), with t taken as 6mm. The stress-strain curves for the flat and corner regions were obtained based on the average material properties parameters given in Table 2 and using the stress-strain model provided in the previous study [30]. Grades of concrete infill as C50, C70 and C90 with nominal f_c of 50, 70 and 90 MPa respectively were used for the parametric studies. Considering these parameters, a total of 27 concrete-filled CFHSS octagonal tubular stub columns were obtained for the parametric studies. The length of each stub column was set to be 3.0 times the D of the cross-section, in consistency with the arrangement applied for experimental investigations.

Through the parametric studies, the behaviour of the structures, including P versus δ responses and $P_{u,FE}$, were predicted. Based on the results, the strength enhancement index (SI) expressed using Eq. (6) and reflecting the contribution of composite action for strength enhancements was estimated. Since no

obvious yield plateau was observed from the stress-strain curves measured for the flat and corner regions of CFHSS octagonal tubes, the $\sigma_{0.2}$ was used in the equation and the subsequent evaluation of design approaches. Effects of B/t ratios and concrete f_c on the SI values were examined, as shown in Figs. 9 (a) and (b). In Fig. 9 (a), it can be observed that the SI decreases with increasing B/t ratios for the structures with the same f_c. As for the structures with the same B/t ratios for their cross-sections, the SI ratio decreases with increasing f_c, as shown in Fig. 9(b). Therefore, strength enhancement due to the beneficial confinement effect is higher for the structures with relatively lower B/t ratios and f_c for concrete infill. These parameters and their effects on the beneficial confinement effect need to be considered and quantified for strength predictions in order to accurately estimate the strength of the structures. The suitable incorporation of effects of these parameters on the strength contribution from steel tube and concrete infill is provided and discussed in more detail in the following section for design approaches.

$$SI = {P_u}/{(\sigma_{0.2}A_s + f_cA_c)} \quad (6)$$

4. Design approaches

Concrete-filled octagonal steel tubular structures are not covered in existing international design codes. Hence, in the current study, the applicability of design approaches given in existing standards for CFST structures with circular and rectangular cross-sections to the concrete-filled CFHSS octagonal tubular stub columns was evaluated. The estimated P_u for the structures based on different standards and approaches proposed by Zhu and Chan [22] and Ahmed and Liang [29] for octagonal CFST stub columns with conventional strength steel were compared with the $P_{u,exp+FE}$ obtained from stub column tests and parametric studies described in Sections 2 and 3 respectively. The results from tests and parametric studies for the design approach evaluation and development cover the structures with S690 high-strength steel, concrete f_c between 50 and 90 MPa, ξ from about 0.3 to 2.77 and B/t ratios from 7.4 to 50. The accuracy of the approaches is discussed in the following sections.

4.1 Eurocode 4

Eurocode 4 [26] provides the specifications for the cross-sectional resistance of rectangular CFST structures under compression as the sum of strength contributed from the steel tube and concrete infill, as expressed in Eq. (7). As for circular cross-section structures, Eqs. (8)-(10) are given in Eurocode 4 and account for the beneficial confinement effect from the circular steel tube. In the equations, D is originally specified as the diameter of circular cross sections and $\bar{\lambda}$ is the relative member slenderness. These equations are specified for the CFST cross-sections satisfying the maximum h/t (rectangular) or D/t (circular) limits without local buckling effect. The h is the height of the rectangular cross sections. Based on the specifications, the $P_{EC,rec}$ and $P_{EC,cir}$ estimated from the equations are compared with the

$P_{u,exp+FE}$ obtained in stub column tests and parametric studies for concrete-filled CFHSS octagonal tubular stub columns, as shown in Fig. 10 and Table 4. While estimating $P_{EC4,cir}$, the D in Eq. (8) was taken as the cross-sectional width for the concrete-filled CFHSS octagonal tubular stub columns, as shown in Fig. 1. As can be seen in the figure and table, slightly conservative strength predictions were obtained based on Eq. (7) while the $P_{EC,cir}$ values are higher than the $P_{u,exp+FE}$ values. The mean of $P_{u,exp+FE}/P_{EC,rec}$ ratios equals to 1.02 with CoV of 0.03 while the mean $P_{u,exp+FE}/P_{EC,cir}$ ratios equals to 0.78 with CoV of 0.07.

$$P_{EC4,rec} = \sigma_{0.2} \times A_s + f_c \times A_c \tag{7}$$

$$P_{EC4,cir} = \eta_{a0}\sigma_{0.2} \times A_s + f_c \times A_c \left[1 + \eta_{c0} \frac{t}{D} \frac{\sigma_{0.2}}{f_c}\right] \tag{8}$$

$$\eta_{a0} = 0.25 \times \left(3 + 2\bar{\lambda}\right) \tag{9}$$

$$\eta_{c0} = 4.9 - 18.5 \times \bar{\lambda} + 17 \times \bar{\lambda}^2 \tag{10}$$

4.2 AISC 360

The AISC 360 [28] also provides specifications for cross-sectional resistance of CFST stub columns under compression. For cross-sections with relatively small h/t (rectangular) or D/t (circular) ratios and classified as compact sections, Eqs. (11) and (12) are given for the structures with rectangular and circular cross-sections, respectively. It shows that no confinement effect is incorporated in the equations and reduction factors of 0.95 and 0.85 are applied to the compressive resistance contributed by the concrete infill. The estimated $P_{AISC,rec}$ and $P_{AISC,cir}$ from the equations are compared with the $P_{u,exp+FE}$ in Fig. 11 and Table 4. Conservative strength predictions were obtained based on Eqs. (11) and (12), as observed in the figure and table. The mean values of $P_{u,exp+FE}/P_{AISC,rec}$ or $P_{u,exp+FE}/P_{AISC,cir}$ ratios are 1.11 and 1.05 with CoV of 0.03 and 0.03, respectively.

$$P_{AISC,rec} = \sigma_{0.2} \times A_s + 0.85 \times f_c \times A_c \tag{11}$$

$$P_{AISC,cir} = \sigma_{0.2} \times A_s + 0.95 \times f_c \times A_c \tag{12}$$

4.3 Approach proposed by Zhu and Chan [22]

An approach was proposed by Zhu and Chan [22] based on the experimental results of octagonal CFST stub columns with conventional strength steel, with the aim to incorporate the confinement effect observed for the structures. The approach was generated by modifying the approach in Eurocode 4 for circular CFST structures and is expressed as Eq. (13). In the equation, D was specified as the cross-sectional width for concrete-filled octagonal steel tubular stub columns. The ultimate

loads $P_{Z\&C}$ predicted using Eq. (13) are compared with the $P_{u,exp+FE}$ in Fig. 12 and Table 4. It can be observed in the figure and table that unconservative strength predictions were obtained. The $P_{Z\&C}$ values are 18% on average higher than the $P_{u,exp+FE}$ values with CoV of 0.05.

$$P_{Z\&C} = \eta_{a0}\sigma_{0.2} \times A_s + f_c \times A_c \left[1 + 0.73 \times \eta_{c0} \frac{t}{D} \frac{\sigma_{0.2}}{f_c}\right] \quad (13)$$

4.4 Approach proposed by Ahmed and Liang [29]

Ahmed and Liang [29] also proposed an approach for octagonal CFST stub columns with conventional strength steel based on the hoop stress (σ_{rp}) provided by the octagonal steel tube to concrete infill for taking into account the beneficial confinement effect. The approach was given using Eqs. (14-16), in which the γ_c is the reduction factor considering the column size effect and D is defined the same as that for the approach from Zhu and Chan [22]. The accuracy of strength predictions ($P_{A\&L}$) obtained using this approach is shown in Fig. 13 and Table 4 in comparison with the $P_{u,exp+FE}$ values. As can be observed in Fig. 13, both conservative and slightly unconservative strength predictions were obtained. The unconservative predictions were mainly obtained for the structures with relatively lower B/t ratios. The mean $P_{u,exp+FE}/P_{A\&L}$ ratios was estimated as 1.02 with CoV of 0.04.

$$P_{A\&L} = \sigma_{0.2} \times A_s + A_c\left[f_c \times \gamma_c + 4.1 \times \sigma_{rp}\right] \quad (14)$$

$$\sigma_{rp} = 3.1963 - 6.8835 \times 10^{-3}\left(\frac{D}{t}\right) \quad (15)$$

$$\gamma_c = 1.85 \times (D - 2t)^{-0.135} \quad (16)$$

4.5 Proposed design approach

The evaluation of existing design approaches shows that the approach from Eurocode 4 for circular CFST structures and the approach proposed by Zhu and Chan [22] provide unconservative strength predictions. Reasonable strength predictions were obtained based on the approach in Eurocode 4 for rectangular CFST structures, the approaches from AISC360 and the approach from Ahmed and Liang [29]. These reasonable strength predictions were estimated by taking the strength contributed from the steel tubular components as the plastic capacity as $\sigma_{0.2} \times A_s$, as shown in Eqs. (7), (11), (12) and (14). However, the stub columns with relatively larger B/t ratios experience local buckling and may have the strength from steel tubes lower than $\sigma_{0.2} \times A_s$.

To study this effect, the strength contributed by steel tube (P_s) to the ultimate load for each concrete-filled CFHSS octagonal tubular stub column investigated in parametric studies was obtained through the FE modelling and normalised by $\sigma_{0.2} \times A_s$. The normalised strengths from steel tubes (η_s) are

plotted with varying B/t in Fig. 14. It can be seen in the figure that the η_s decreases with increasing B/t ratios and is lower than 1.0 for relatively larger B/t ratios. At each B/t ratio, the variation of η_s for structures with different f_c values is quite limited. The strength contributed by concrete infill (P_c) to the ultimate load of each concrete-filled CFHSS octagonal tubular stub column was also obtained through FE modelling and normalised by $f_c \times A_c$. The normalised strengths from concrete infill (η_c) that count the confinement effect are plotted with varying B/t in Fig. 15 (a). It can be observed that the η_c decreases with increasing B/t ratios. For the same B/t ratio, the η_c obtained for the structures with different f_c are also different. To quantify the effect of f_c on η_c, the η_c is also plotted against f_c in Fig. 15(b), showing that η_c decreases with increasing f_c.

In order to more accurately incorporate the contribution of P_s and P_c to the ultimate loads of the structures, the approach describing the strength contributions from different components forming the structures is proposed, as expressed as Eq. (17). Eqs. (18) and (19) for η_s and η_c respectively were obtained through regression analysis based on the P_s and P_c with the effects of B/t and f_c taken into consideration, as shown in Fig. 16 (a) and (b) for the agreements of the equations with those results from FE modelling. To estimate η_c using Eq. (19), f_c in the unit of MPa should be used. The strength predictions (P_{pro}) estimated using Eqs. (17)-(19) are compared with the $P_{u,exp+FE}$ in Fig. 17 and Table 4. The comparison shows that the P_{pro} are in excellent agreement with $P_{u,exp+FE}$. The mean value of $P_{u,exp+FE}/P_{pro}$ ratios is 1.00 with CoV of 0.02. Comparing with the design approaches in standards and those from literature, the proposed approach counts the strength contributed from steel tubes and concrete infill, and overall, provides accurate strength predictions.

$$P_{pro} = P_s + P_c = \eta_s \times \sigma_{0.2} \times A_s + \eta_c \times f_c \times A_c \quad (17)$$

$$\eta_s = 1 - 0.063 \times \ln\left(0.12 \times \frac{B}{t}\right) \quad (18)$$

$$\eta_c = 1 + \left(\frac{t}{B \times f_c}\right)^{0.35} \quad (19)$$

5. Conclusions

Behaviour of concrete-filled CFHSS octagonal tubular stub columns under axial compression was investigated in this study through experiments and numerical modelling. Three CFHSS octagonal tubular stub column specimens and twelve concrete-filled CFHSS octagonal tubular stub column specimens with varying plate width-to-thickness ratios were tested. The test results of ultimate loads, load versus end-shortening and failure modes are reported. In addition to the experimental investigation, numerical modelling was performed on the concrete-filled CFHSS octagonal tubular stub columns with various plate width-to-thickness ratios and cylinder compressive strengths for

concrete infill using the validated FE model. The numerical modelling shows that the strength enhancement is higher for the stub columns with relatively lower B/t and f_c.

The obtained results from stub column tests and parametric studies were employed to evaluate the applicability of existing design approaches for cross-sectional resistance in European and American standards and that proposed by Zhu and Chan [22] and Ahmed and Liang [29]. Based on the approach in Eurocode 4 for circular CFST structures and the approach from Zhu and Chan [22], the ultimate loads were overestimated by 18-28%. The evaluation shows that conservative strength predictions on average were obtained based on the design approach for rectangular concrete-filled steel tubular structures in Eurocode 4, approaches in AISC 360 and the approach from Ahmed and Liang [29]. Although conservative strength predictions were obtained based on these approaches, the approaches take the strength from steel tubes as the plastic resistance which was found to be higher than the strength from steel tubes estimated in parametric studies for the concrete-filled CFHSS octagonal tubular stub columns. An approach describing the strength contributed from steel tube and concrete infill was proposed and can be applied to obtain more accurate and less scattered strength predictions for the concrete-filled CFHSS octagonal tubular stub columns in structural design.

Acknowledgements

The research work presented in this paper was supported by a grant from the Research Grants Council of the Hong Kong Special Administrative Region, China (Project no. 152492/16E). The authors would like to thank Mr. Ho Yeung Man, who helped in undertaking the tests reported in this paper as part of his undergraduate project. The authors would also like to appreciate the support from the Chinese National Engineering Research Centre for Steel Construction (Hong Kong Branch) at The Hong Kong Polytechnic University.

References

[1] Han, L.H., Li, W. and Bjorhovde, R. 2014. Developments and advanced applications of concrete-filled steel tubular (CFST) structures: members. *Journal of Constructional Steel Research*, 100, 211-228.

[2] Huang, W.J., Lai, Z.C., Chen, B.C., Xie, Z.T. and Varma, A.H. 2018. Concrete-filled steel tube (CFT) truss girders: experimental tests, analysis, and design. *Engineering Structures*, 156, 118-129.

[3] Wang, Z.B., Tao, Z., Han, L.H., Uy, B., Lam, D. and Kang, W.H. 2017. Strength, stiffness, and ductility of concrete-filled steel columns under axial compression. *Engineering Structures*, 135, 209-221.

414 [4] Chen, J.B. and Chan, T.M. 2019. Experimental assessment of the flexural behaviour of concrete-
415 filled steel tubular beams with octagonal sections. *Engineering Structures*, 199, 109604.

416 [5] Lai, Z.C., Varma, A.H. and Griffis, L.G. 2016. Analysis and design of noncompact and slender
417 CFT beam-columns. *Journal of Structural Engineering*, 142(1), 04015097.

418 [6] Xiong, M.X., Xiong, D.X. and Liew, J.Y.R. 2017. Axial performance of short concrete filled steel
419 tubes with high- and ultra-high-strength materials. *Engineering Structures*, 136, 494-510.

420 [7] Uy, B. 2000. Strength of concrete filled steel box columns incorporating local buckling. *Journal of*
421 *Structural Engineering*, 126(3), 341-352.

422 [8] O'Shea, M.D. and Bridge, R.Q. 2000. Design of circular thin-walled concrete filled steel tubes.
423 *Journal of Structural Engineering*, 126(11), 1295-1303.

424 [9] Ellobody, E. and Young, B. 2006. Nonlinear analysis of concrete-filled steel SHS and RHS
425 columns. *Thin-Walled Structures*, 44, 919-930.

426 [10] Thai, S., Thai, H.T., Uy, B. and Ngo, T. 2019. Concrete-filled steel tubular columns: test
427 database, design and calibration. *Journal of Constructional Steel Research*, 157, 161-181.

428 [11] Chen, J.B., Chan, T.M. and Chung, K.F. 2021. Design of square and rectangular CFST cross-
429 sectional capacities in compression. *Journal of Constructional Steel Research*, 176, 106419.

430 [12] Fang, H., Chan, T.M. and Young, B. 2018. Structural performance of cold-formed high strength
431 steel tubular columns. *Engineering Structures*, 177, 473-488.

432 [13] Uy, B. 2018. Applications, behavior, and construction of high performance steels in steel-
433 concrete composite structures. *Proceedings of 12th International Conference on advances in Steel-*
434 *Concrete Composite Structures*, València, Spain, 91-97.

435 [14] Fang, H. and Chan, T.M. 2019. Buckling resistance of welded high-strength-steel box-section
436 members under combined compression and bending. *Journal of Constructional Steel Research*, 162,
437 105711.

438 [15] Ke, K., Yam, M.C.H., Zhang, H.Y., Lam, A.C.C. and Zhou, X.H. 2020. High-strength steel
439 frames with SMA connections in self-centring energy-dissipation bays: insights and a multimodal
440 nonlinear static procedure. *Smart Materials and Structures*, 29, 125020.

[16] Li, X.Y., Zhang, J.W. and Cao, W.L. 2020. Hysteretic behavior of high-strength concrete shear walls with high-strength steel bars: experimental study and modelling. *Engineering Structures*, 214, 110600.

[17] Su, M.N., Cai, Y.C., Chen, X.R. and Young, B. 2020. Behaviour of concrete-filled cold-formed high strength steel circular stub columns. *Thin-Walled Structures*, 157, 107078.

[18] Patel, V.I., Hassanein, M.F., Thai, H.T., Al Abadi, H., Elchalakani, M. and Bai, Y. 2019. Ultra-high strength circular short CFST columns: axisymmetric analysis, behavior and design. *Engineering Structures*, 179, 268-283.

[19] Yan, J.B., Chen, A.Z. and Zhu, J.S. 2020. Behaviours of square UHPFRC-filled steel tubular stub columns under eccentric compression. *Thin-Walled Structures*, 107222.

[20] Huang, Z.C., Uy, B., Li, D.X. and Wang, J. 2020. Behaviour and design of ultra-high-strength CFST members subjected to compression and bending. *Journal of Constructional Steel Research*, 175, 106351.

[21] Khan, M., Uy, B., Tao, Z. and Mashiri, F. 2017. Concentrically loaded slender square hollow and composite columns incorporating high strength materials. *Engineering Structures*, 131, 69-89.

[22] Zhu, J.Y. and Chan, T.M. 2018a. Experimental investigation on octagonal concrete filled steel stub columns under uniaxial compression. *Journal of Constructional Steel Research*, 147, 457-467.

[23] Tomii, M., Yoshimura, K. and Morishita, Y. 1977. Experimental studies on concrete-filled steel tubular stub columns under concentric loading. *International colloquium on stability of structures under static and dynamic loads*, Washington DC, May 17–19, 1977. p. 718–41.

[24] Ding, F.X., Li, Z., Cheng, S.S. and Yu, Z.W. 2016. Composite action of octagonal concrete-filled steel tubular stub columns under axial loading. *Thin-Walled Structures*, 107, 453-461.

[25] Hassanein, M.F., Patel, V.I., Elchalakani, M. and Thai, H.T. 2018. Finite element analysis of large diameter high strength octagonal CFST short columns. *Thin-Walled Structures*, 123, 467-482.

[26] EN1994-1-1. (2004) *Eurocode 4: Design of Composite Steel and Concrete Structures-Part1-1: General Rules and Rules for Buildings*, European Committee for Standardization.

[27] Zhu, J.Y. and Chan, T.M. 2018b. Behaviour of polygonal-shaped steel-tube columns filled with high-strength concrete. *Structures and Buildings*, 171, 96-112.

[28] ANSI/AISC 360-16, 2016. *Specification for structural steel buildings*. AISC, Chicago.

[29] Ahmed, M. and Liang, Q.Q. 2021. Numerical modelling of octagonal concrete-filled steel tubular short columns accounting for confinement effects. *Engineering Structures*, 226, 111405.

[30] Fang, H., Chan, T.M. and Young, B. 2018. Material properties and residual stresses of octagonal high strength steel hollow sections. *Journal of Constructional Steel Research,* 148, 479-490.

[31] Fang, H., Chan, T.M. and Young, B. 2019. Behavior of octagonal high-strength steel tubular stub columns. *Journal of Structural Engineering*, 145(12), 04019150.

[32] Fang, H., Chan, T.M. and Young, B. 2021. Experimental and numerical investigations of octagonal high-strength steel tubular stub columns under combined compression and bending. *Journal of Structural Engineering*, 147(1), 04020282.

[33] Wang, F.Y., Young, B. and Gardner, L. 2020. CFDST sections with square stainless steel outer tubes under axial compression: Experimental investigation, numerical modelling and design. *Engineering Structures*, 207, 110189.

[34] Chen, J.B., Fang, H. and Chan, T.M. 2021. Design of fixed-ended octagonal shaped steel hollow sections in compression. *Engineering Structures*, 111520.

[35] Fang, H. and Chan, T.M. 2019. Resistance of axially loaded hot-finished S460 and S690 steel square hollow stub columns at elevated temperatures. *Structures*, 17, 66-73.

[36] Song, Q.Y., Han, L.H., Zhou, K. and Feng, Y. 2018. Fire resistance of circular-filled steel tubular (CFST) column protected by intumescent coating. *Journal of Constructional Steel Research*, 147, 154-170.

[37] Sheehan, T, Dai, X.H., Chan, T.M. and Lam, D. 2012. Structural response of concrete-filled elliptical steel hollow sections under eccentric compression. *Engineering Structures*, 45, 314-323.

[38] ABAQUS [Computer software] (2014). Dassault Systèmes, Providence, RI.

[39] ACI 318, 2014. *Building code requirements for structural concrete and commentary*. Farmington Hills, MI, USA.

[40] Cai, Y.C., Quach, W.M. and Young, B. 2019. Experimental and numerical investigation of concrete-filled hot-finished and cold-formed steel elliptical tubular stub columns. *Thin-Walled Structures*, 145, 106437.

[41] Han, L.H., Yao, G.H. and Tao, Z. 2007. Performance of concrete-filled thin-walled steel tubes under pure torsion. *Thin-Walled Structures*, 45, 24-36.

[42] Tao, Z., Wang, Z.B. and Yu, Q. 2013. Finite element modelling of concrete-filled steel stub columns under axial compression. *Journal of Constructional Steel Research*, 89, 121-131.

[43] Papanikolaou, V.K. and Kappos, A.J. 2007. Confinement sensitive plasticity constitutive model for concrete in triaxial compression. *International Journal of Solids and Structures*, 44 (21), 7021-7048.

[44] Yu, T., Teng, J.G., Wong, Y.L. and Dong, S.L. 2010. Finite element modelling of confined concrete I: drucker-Prager type plasticity model. *Engineering Structures*, 32 (3), 665-679.

[45] Bazˇant, Z.P. and Becq-Giraudon, E. 2002. Statistical prediction of fracture parameters of concrete and implications for choice of testing standard. *Cement and Concrete Research*, 32, 529-556.

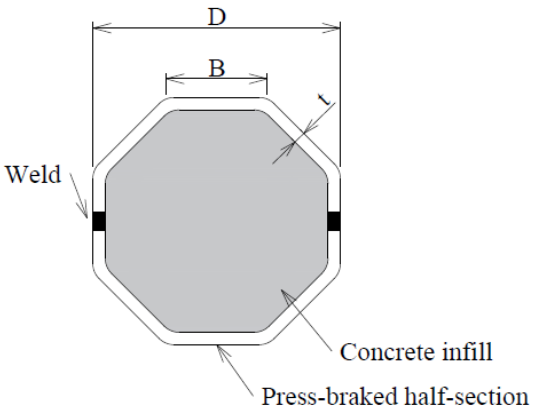

Fig. 1. Concrete-filled CFHSS Octagonal tubular stub column cross-section.

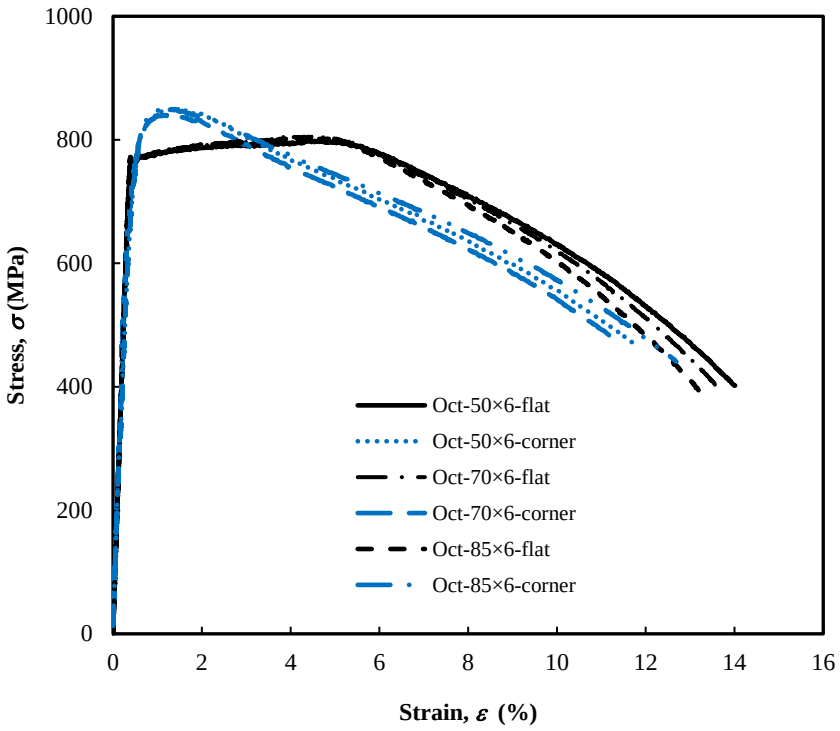

Fig. 2. Measured stress-strain curves for CFHSS octagonal tubes [32].

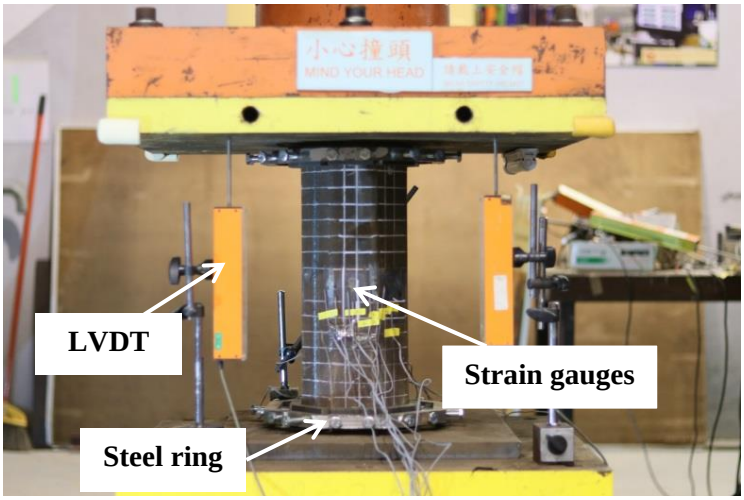

Fig. 3. Test set-up for a stub column specimen.

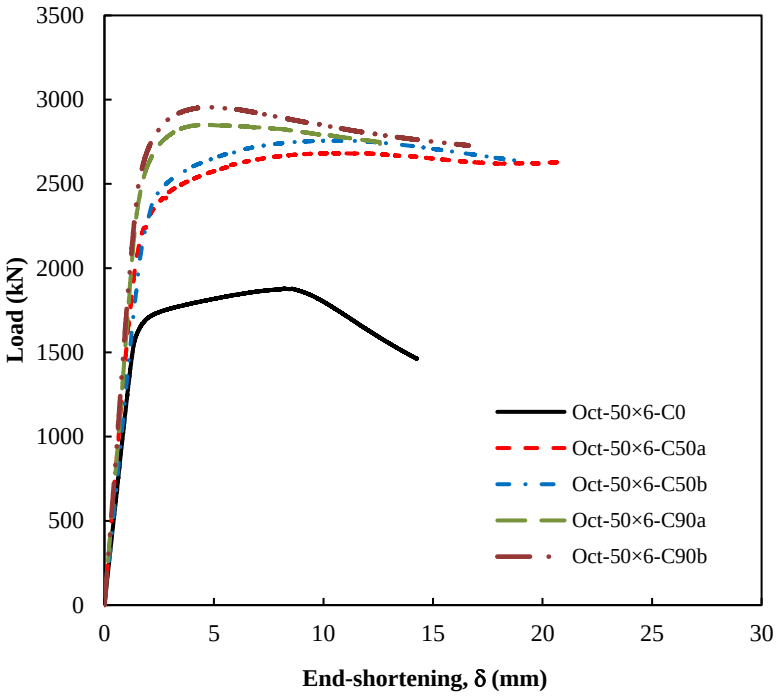

(a) Oct-50×6 specimens with different concrete grades

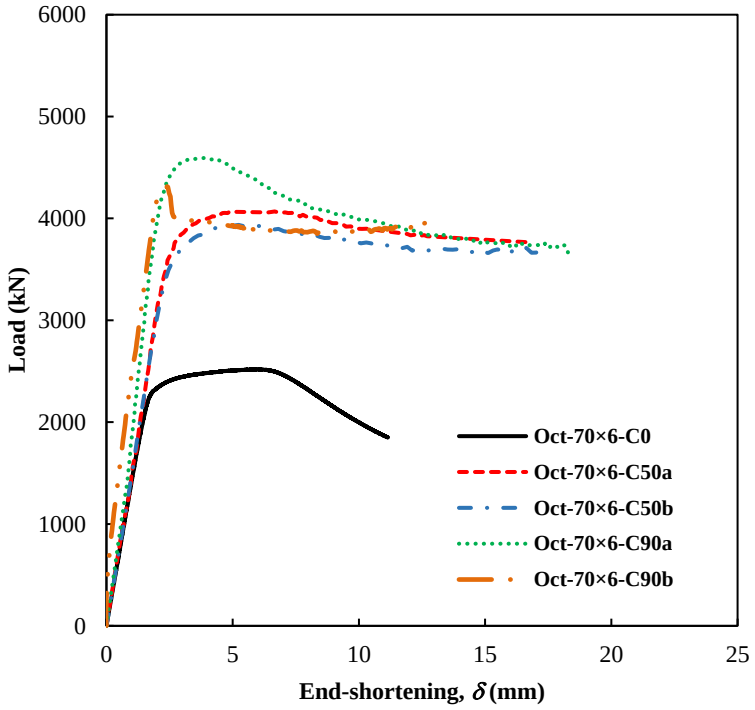

(b) Oct-70×6 specimens with different concrete grades

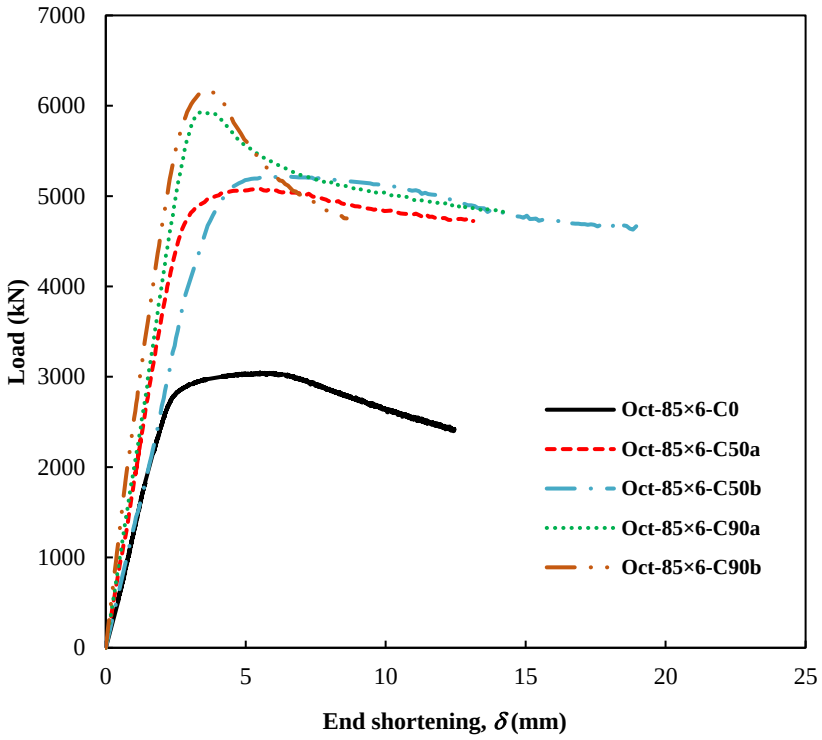

(c) Oct-85×6 specimens with different concrete grades

Fig. 4. Load versus end-shortening curves obtained for different specimens during stub column tests.

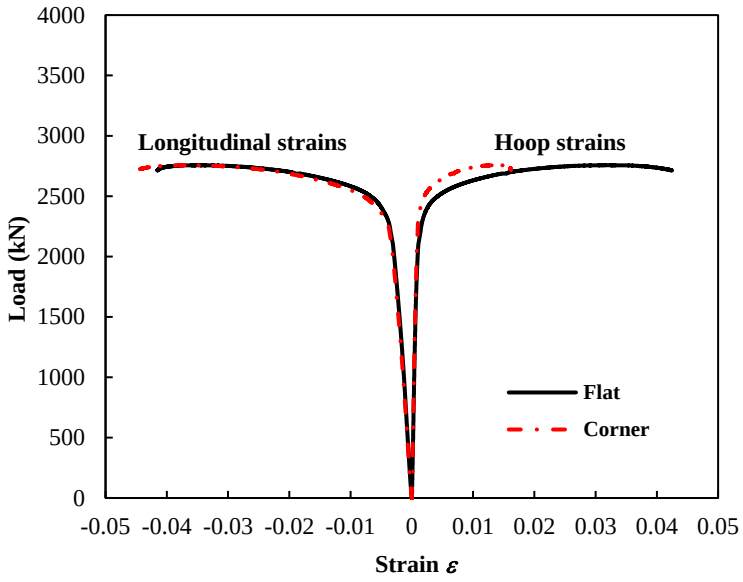

(a) Oct-50×6-C50b

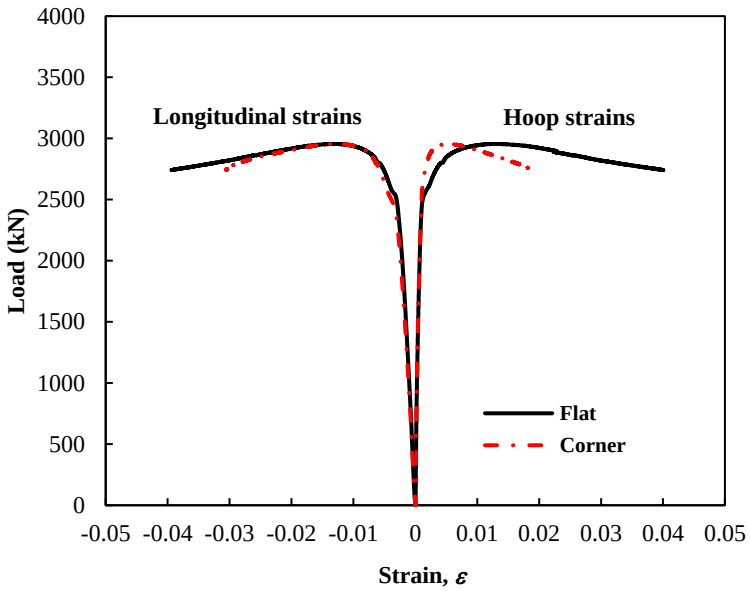

(b) Oct-50×6-C90b

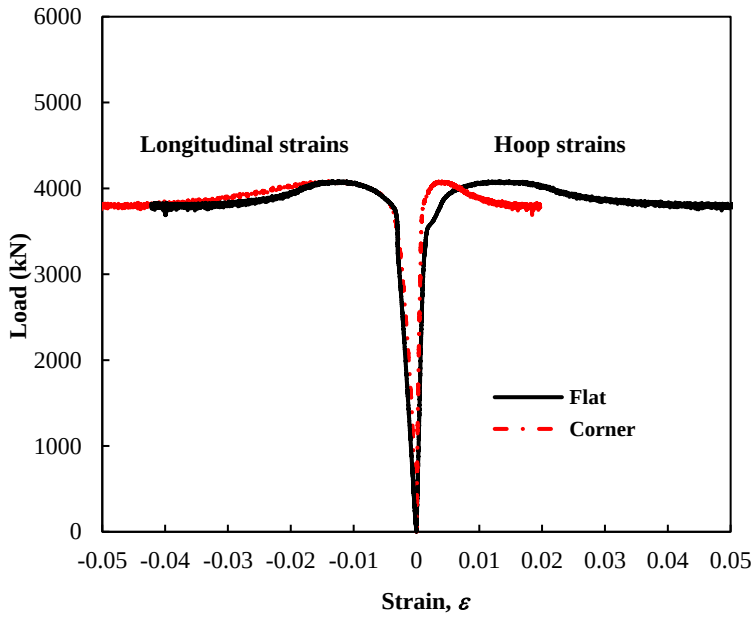

(c) Oct-70×6-C50a

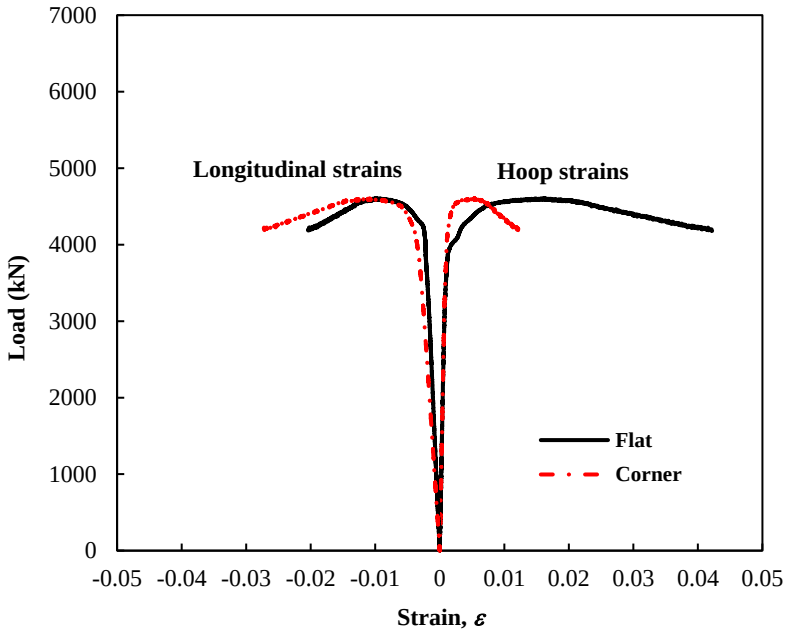

(d) Oct-70×6-C90a

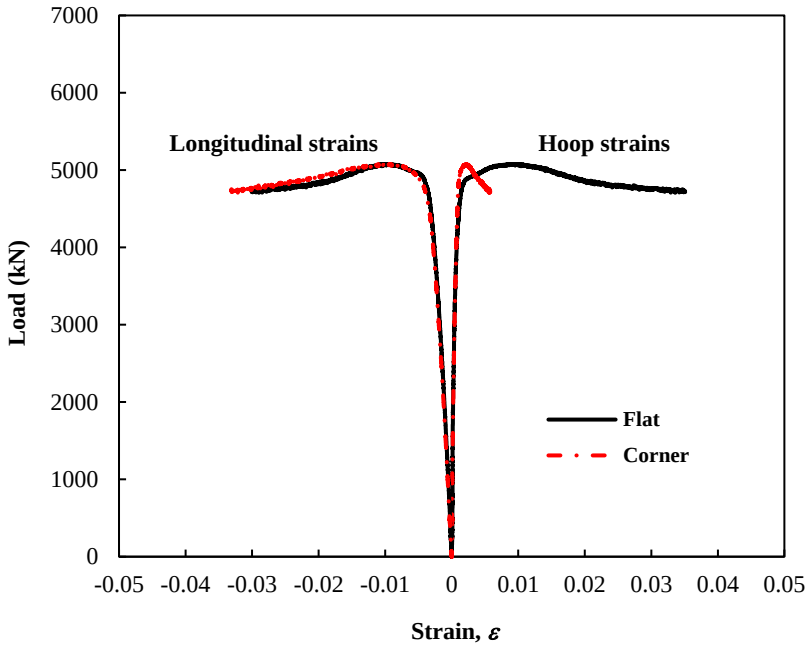

(e) Oct-85×6-C50a

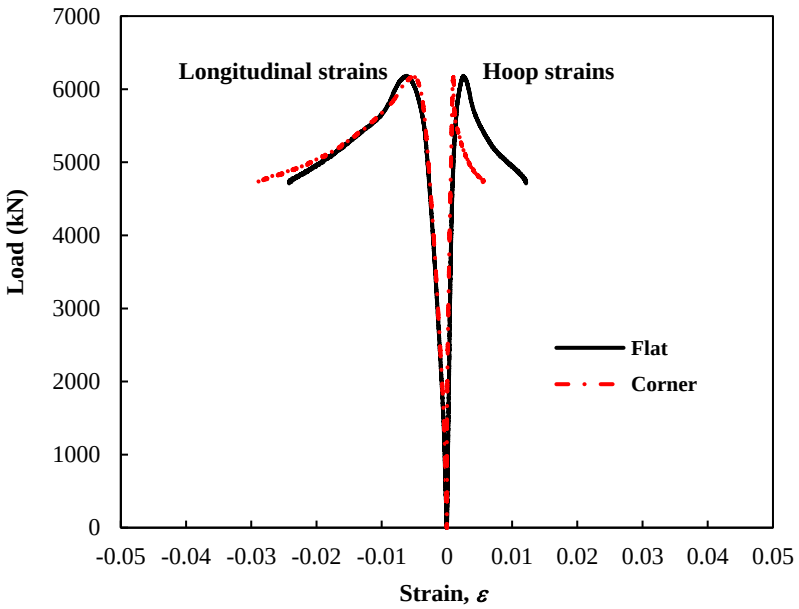

(f) Oct-85×6-C90b

Fig. 5. Load versus longitudinal and hoop strain curves for different octagonal CFST stub columns.

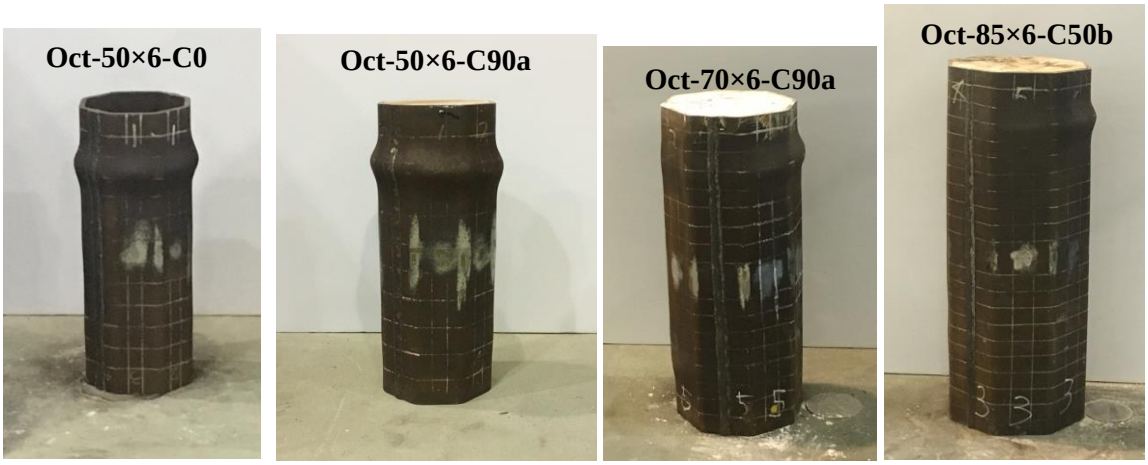

Fig. 6. Failure modes of typical stub column specimens.

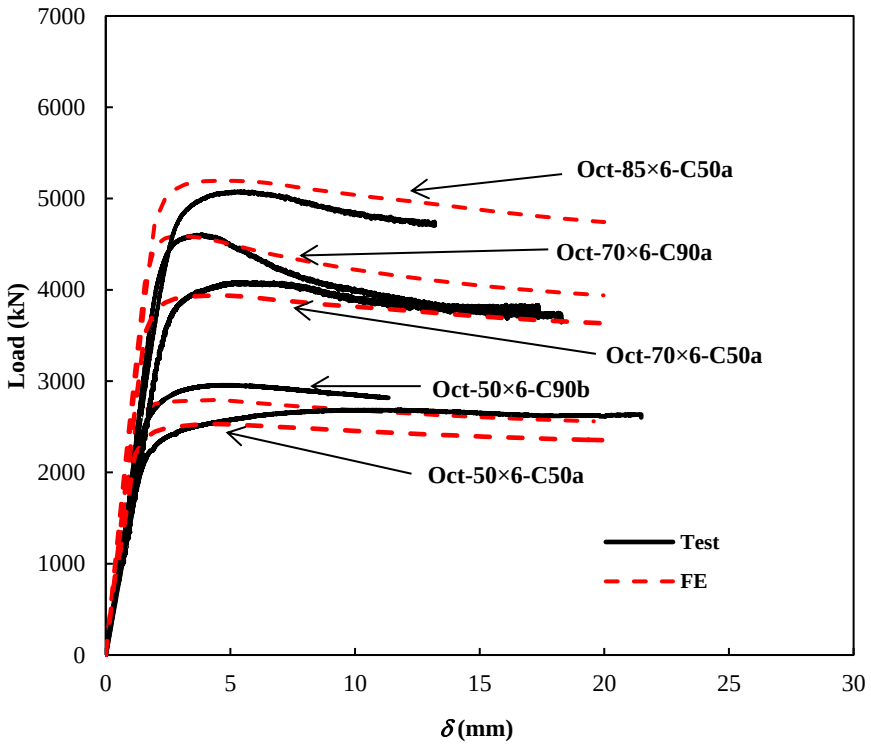

Fig. 7. Comparison of load versus δ predicted in FE modelling with results of stub column tests.

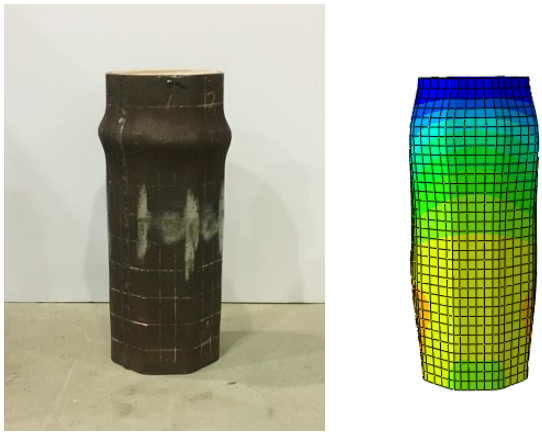

Fig. 8. Comparison of failure mode predicted in FE modelling with the experimental result for Oct-50×6-C90a.

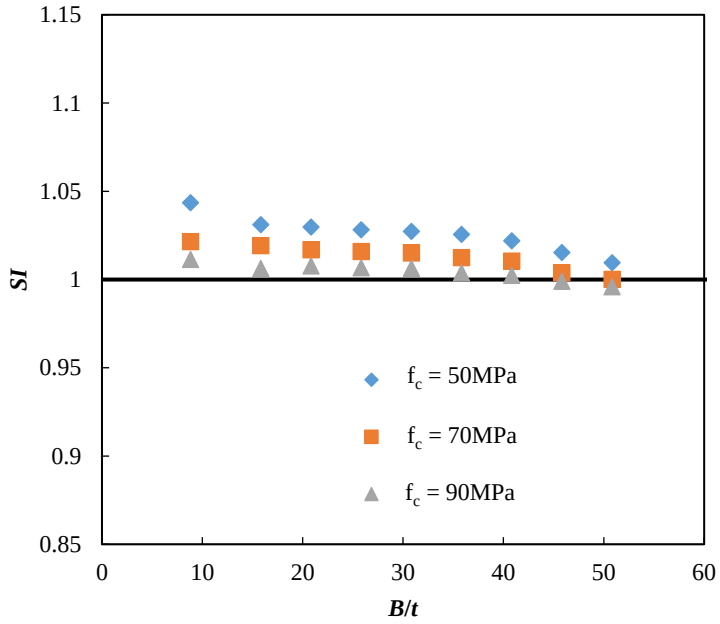

(a)

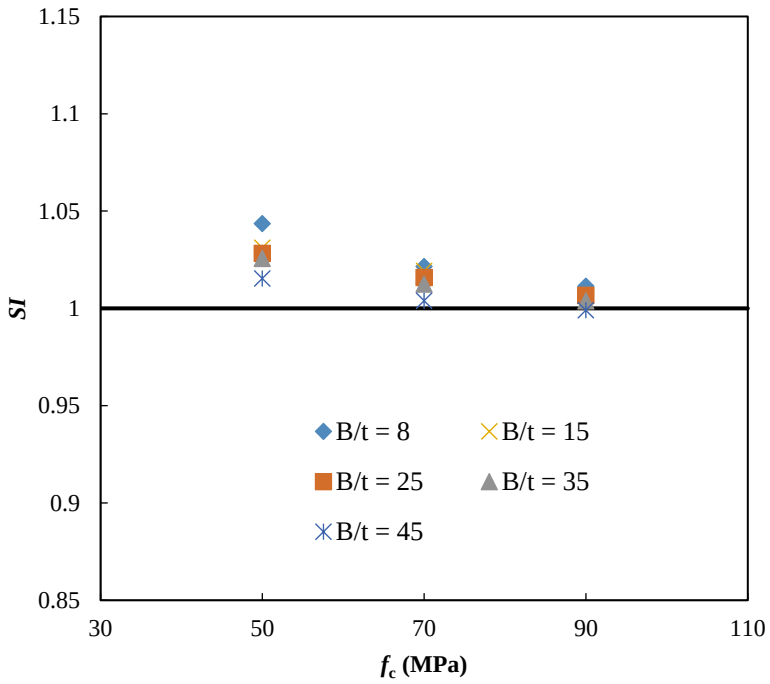

(b)

Fig. 9. Variation of *SI* values with (a) *B*/*t* ratios; (b) f_c of concrete infill.

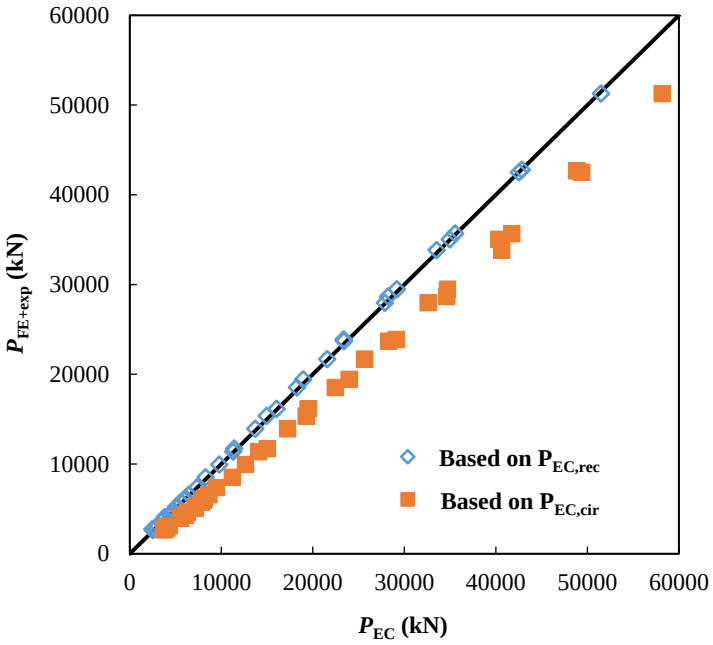

Fig. 10. Comparison of strength predictions based on Eurocode 4 with the experimental and FE results.

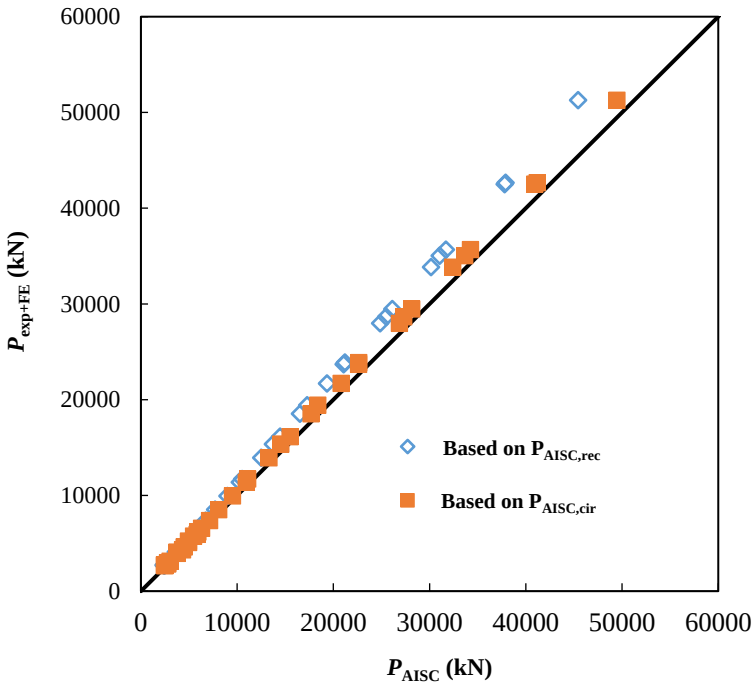

Fig. 11. Comparison of strength predictions based on AISC 360 with the experimental and FE results.

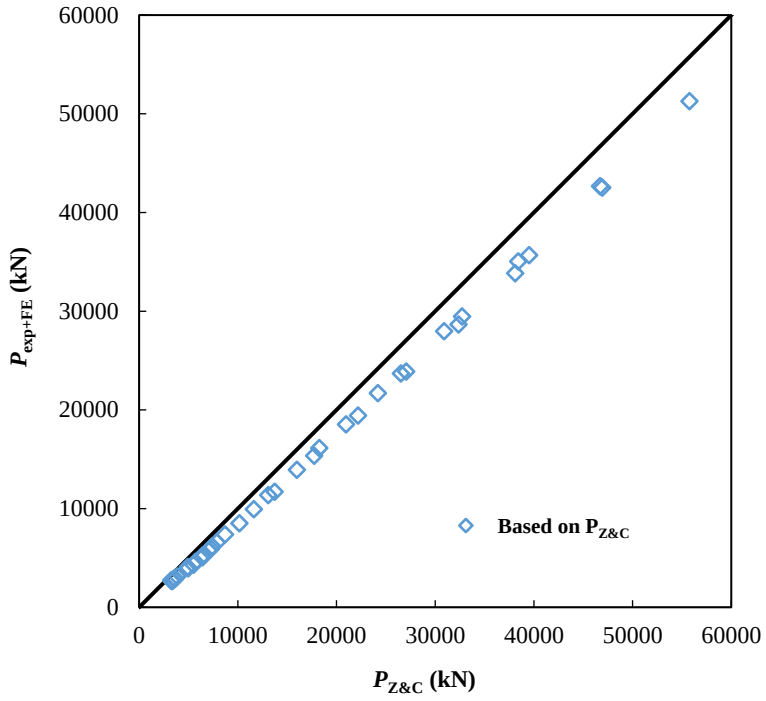

Fig. 12. Comparison of strength predictions based on the approach proposed by Zhu and Chan [22] with the experimental and FE results.

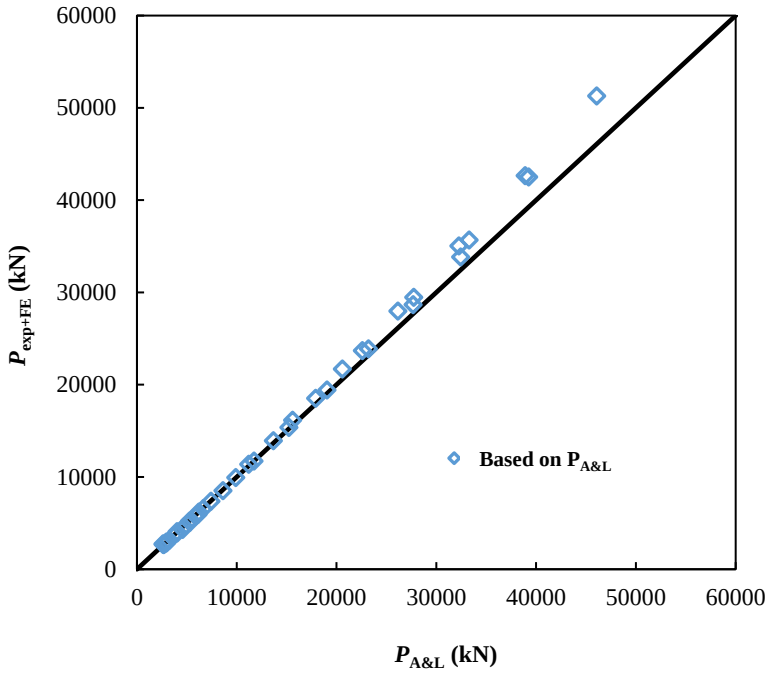

Fig. 13. Comparison of strength predictions based on the approach proposed by Ahmed and Liang [29] with the experimental and FE results.

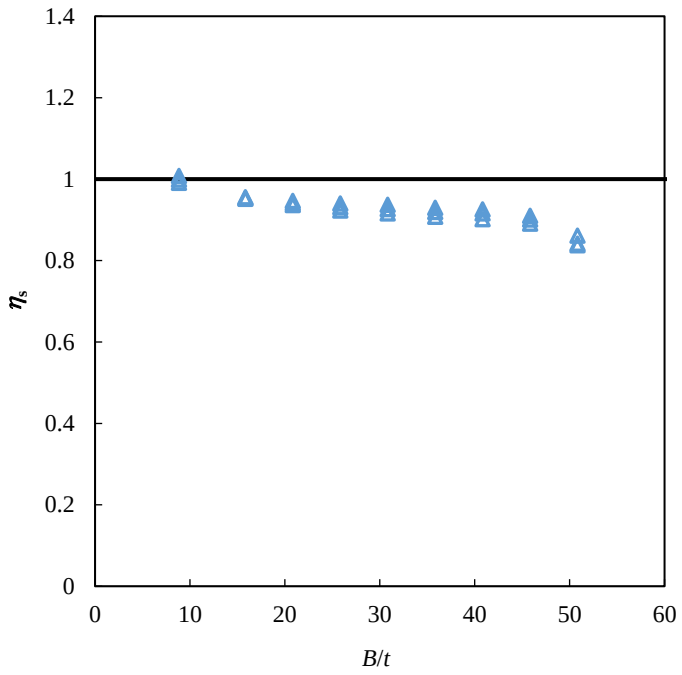

Fig. 14. Variation of η_s with B/t ratios.

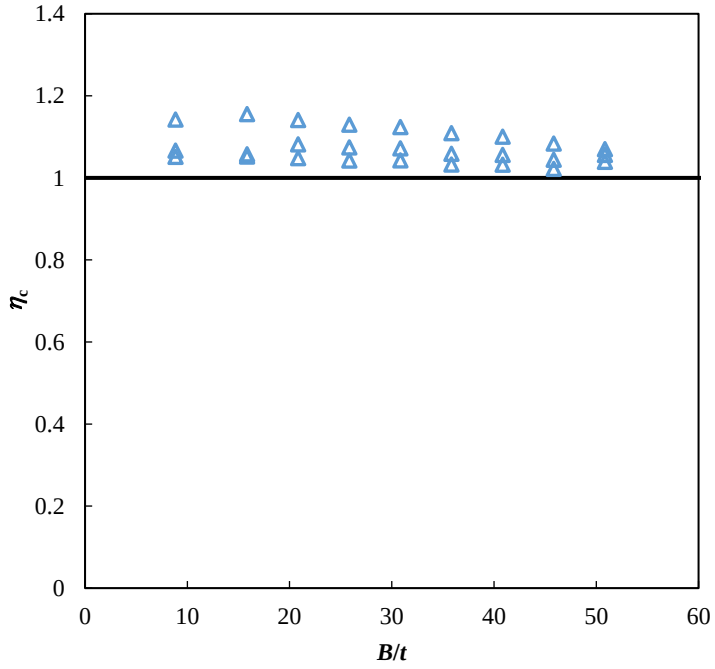

(a)

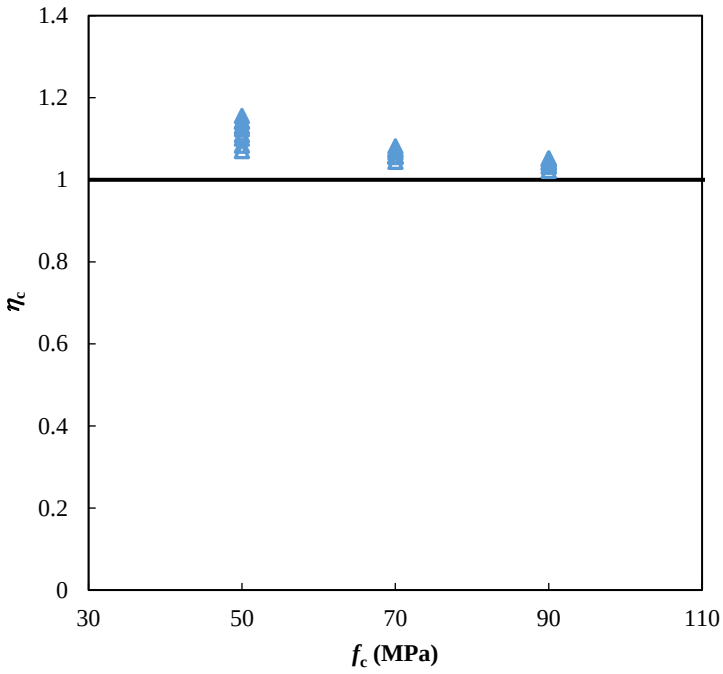

(b)

Fig. 15. Variation of η_c with (a) B/t ratios and (b) f_c.

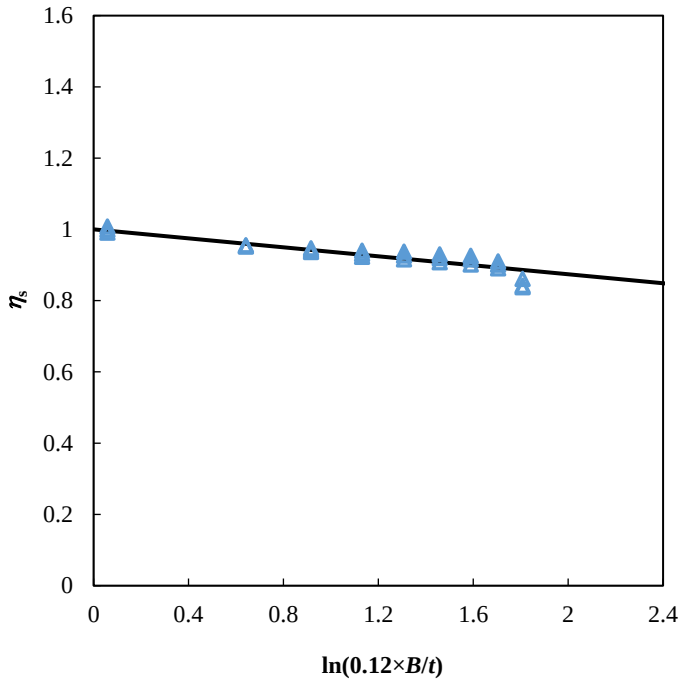

(a)

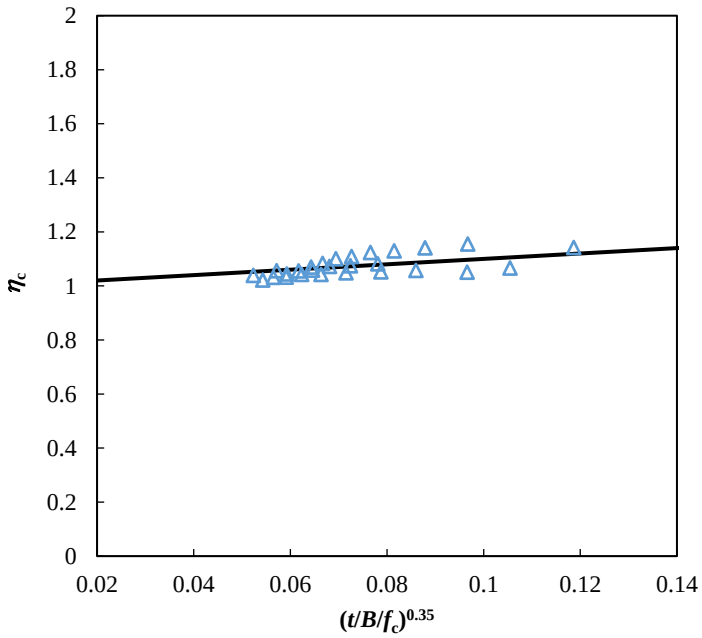

(b)

Fig. 16. Comparison of (a) η_s and (b) η_c estimations using Eqs. (18) and (19) respectively with that obtained based on parametric studies results.

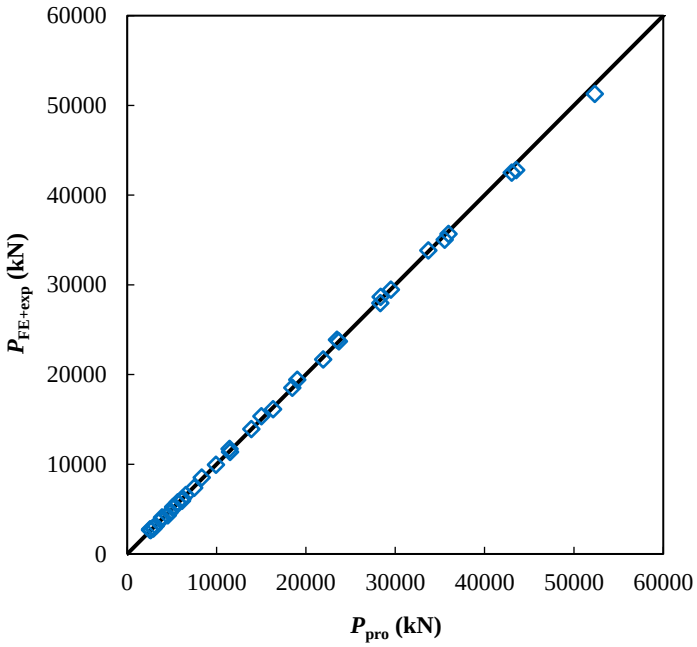

Fig. 17. Comparison of strength predictions based on the proposed approach with the experimental and FE results.